$WO_2...(NaOZ)_2$ to yield the W_2O_6 dimer products $(ZONa)...O_2W(\mu\text{-}O)_2WO_2...(NaOZ)$. A similar type of reaction can therefore be envisaged for the "one step" thermal oxidation of $n[WO_2]$-$Na_{56}Y$ with O_2 at 300 °C to yield $n[WO_3]$-$Na_{56}Y$ (Figure 10).

The "two-step" vacuum thermal reduction of $n[WO_3]$-$Na_{56}Y$ to $n[WO_{2.5}]$-$Na_{56}Y$ and then to $n[WO_2]$-$Na_{56}Y$ is a much more difficult process to envision. The mechanism could be different for the low and high loading regimes. In the former case, both homo- and heterolytic $W(\mu\text{-}O)_2W$ bridge cleavage reactions of the W_2O_6 dimer are possible, leading to anchored WO_3 and WO_2 monomers (the former expected to be more labile than the latter), which could then participate in bimolecular encounters to yield W_2O_5 dimers, and then similarly on to anchored WO_2 monomers. In the latter case, bimolecular encounters between W_2O_6 dimers could result in O_2 loss from the $W^{6+}(\mu\text{-}O)_2W^{6+}$ bridge and formation of W_2O_5 dimers, a process which then repeats to yield WO_2 monomers. Spectroscopic and kinetic studies are underway, using extensive $^{12}C/^{13}C$ and $^{16}O/^{17}O/^{18}O$ isotopic labeling techniques, to quantitatively assess some of the mechanistic ideas discussed above.

Conclusions

A clean, mild, and quantitative photoinduced oxidative transformation of precursor $n[W(CO)_6]$-$Na_{56}Y$ in the presence of O_2 yields $n[WO_3]$-$Na_{56}Y$. Sequential saturation-filling photooxidation reactions allow one to essentially achieve full filling of $n \approx 32$ for the encapsulated WO_3 unit. Subsequent vacuum thermal treatments of $n[WO_3]$-$Na_{56}Y$ cause O_2 loss, which provides access to $n[WO_{3-x}]$-$Na_{56}Y$ materials in which one can systematically manipulate the oxygen content and structural and electronic properties of the imbibed WO_{3-x} guests over the entire composition field $0 < n \leq 32$ and $0 \leq x \leq 1$.

A multiprong approach to the structural characterization of these materials has revealed that well-defined monomeric, dimeric, and tetrameric molecular tungsten oxides WO_{3-x} exist in the α-cages of the $Na_{56}Y$ host for specific values of n and x: Na^+ cation anchored W_2O_6 dimers when $x = 0$ and $n = 16, 28, 32$; Na^+ cation anchored W_2O_5 dimers when $x = 0.5$ and $n = 16$; Na^+ cation anchored W_4O_{10} tetramers when $x = 0.5$ and $n = 32$; and Na^+ and oxygen framework anchored WO_2 monomers when $x = 1$ and $n = 16, 28, 32$.

Depending on the degree of filling of the α-cage void volume by these WO_{3-x} units, one can visualize them as either *isolated* or *coupled* within a molecular orbital or miniband[33] type description of their electronic properties.

For the special case of half- ($n = 16$) and full-filling ($n = 32$) of the "parent" $n[WO_3]$-$Na_{56}Y$, the available information suggests that these materials can be considered to be intrazeolite tungsten(VI) oxide supralattices, built up of α-cage W_2O_6 dimers at $n = 16$ and W_2O_6 *dimers-of-dimers* at $n = 32$. Intra- and intercavity coupling between W_2O_6 dimers provides one with a miniband type description of the electronic properties of these materials, Figures 12 and 13. In this view of the materials, one can consider that the thermal reductive-elimination of O_2 from $n[WO_3]$-$Na_{56}Y$ provides a simple chemical means of injecting variable numbers of electrons into an ordered array of electronically coupled W_2O_6 units. Thus one can precisely control the oxidation state, degree of n-doping, and extent of miniband filling of a tungsten(VI) oxide supralattice. This approach may prove valuable if these kinds of materials are ever to find application in catalysis, solid-state chemistry, and materials science.

Acknowledgment. We acknowledge the National Sciences and Engineering Research Council of Canada's Operating and Strategic Grants Programmes for generous financial support of this work. S.Ö. expresses his gratitude to the Middle East Technical University, Ankara, for granting him an extended leave of absence to conduct his research at the University of Toronto. Valuable discussion with and the assistance of Dr. Peter Macdonald (MAS-NMR), Mr. Raz Jelinek, Dr. Alex Pines (DOR-NMR), Dr. Heinz Robota, Dr. Karin Moller, Dr. Thomas Bein (EXAFS), Dr. Galen Stucky, Dr. W. Harrison (PXRD), Dr. Ross Davidson (XPS), and Dr. Neil Coombs (TEM, STEM-EDX) with various aspects of this project is most deeply appreciated. Research was carried out, in part, at the National Synchrotron Light Source, Brookhaven National Laboratory, Upton, NY, which is supported by the United States Department of Energy.

Metal-Metal vs Tellurium-Tellurium Bonding in WTe_2 and Its Ternary Variants $TaIrTe_4$ and $NbIrTe_4$

Arthur Mar, Stéphane Jobic,† and James A. Ibers*

Contribution from the Department of Chemistry and Science and Technology Center for Superconductivity, Northwestern University, Evanston, Illinois 60208-3113.
Received February 27, 1992

Abstract: The new ternary transition-metal tellurides $TaIrTe_4$ and $NbIrTe_4$ are ordered variants of the WTe_2 structure, which in turn is based on a distortion of the CdI_2-type layered structure. The layers in WTe_2 consist of buckled sheets of Te atoms, with the metal atoms residing in distorted octahedral sites. Through single-crystal X-ray diffraction methods, the structure of $TaIrTe_4$ has been determined and that of WTe_2 has been redetermined. The compounds $TaIrTe_4$ and WTe_2 belong to the space group C_{2v}^7-$Pmn2_1$ of the orthorhombic system with four formula units in cells of dimensions $a = 3.770$ (1), $b = 12.421$ (6), and $c = 13.184$ (6) Å and $a = 3.477$ (2), $b = 6.249$ (4), and $c = 14.018$ (9) Å, respectively, at 113 K. While metal-metal bonding is a structural feature common to all three compounds, Te-Te bonding is observed only in the ternary compounds. The trends of increasing metal-metal and decreasing Te-Te distances on progressing from WTe_2 to $TaIrTe_4$ and $NbIrTe_4$ have been rationalized by electronic band (extended Hückel) calculations. These trends are related to the creation of Te-Te bonds, ensuring the stability of the WTe_2 structure type even when addition of more d electrons leads to a weakening of metal-metal bonds. This concept is generalized to an entire series of compounds $MM'Te_4$ (M = Nb, Ta; M' = Ru, Os, Rh, Ir).

Introduction

In the past two decades, the synthetic chemistry of transition-metal chalcogenides has developed rapidly, primarily because these compounds are found to possess a rich structural chemistry[1] and a wide variety of unusual physical properties. These properties, associated with the anisotropic character inherent in these compounds, include charge density waves[2-9] and superconductivity.[10-14]

† Permanent address: Institut des Matériaux de Nantes, Laboratoire de Chimie des Solides, 2, rue de la Houssinière, 44072 Nantes, Cédex 03, France.

(1) *Crystallography and Crystal Chemistry of Materials with Layered Structures*; Lévy, F., Ed.; Physics and Chemistry of Materials with Layered Structures 2; D. Reidel: Dordrecht, Holland, 1976.

0002-7863/92/1514-8963$03.00/0

Until recently,[15-30] the tellurides had received much less attention than the sulfides and selenides. The more covalent character of tellurium, relative to its lighter congeners, endows its compounds with properties and structures that are often strikingly distinct from the sulfides and selenides. Thus, there are stoichiometries observed in the tellurides that have not been found in the sulfides and selenides, and vice versa. NbQ_3 is known for Q = S and Se[31-33] but not for Q = Te, while NbQ_4 exists for Q = Te[34,35] but must be stabilized as $(NbQ_4)I_{0.33}$ for Q = Se.[36] Coordination geometries are sometimes different even among compounds with identical stoichiometry. In NbQ_2, Nb is in a trigonal prismatic coordination for Q = S and Se but in a distorted octahedral coordination for Q = Te.[1,37]

The increased covalency of tellurium leads to greater variability in chalcogen–chalcogen bonding among the tellurides.[38-40] Under similar chemical conditions, sulfur and selenium tend to take on the oxidation state of 1- and form local $(Q–Q)^{2-}$ pairs (typical bond lengths are 2.05 Å for $(S–S)^{2-}$[41,42] and 2.35 Å for $(Se–Se)^{2-}$[43,44]), while tellurium has a propensity to adopt oxidation states intermediate between 1- and 2- that lead to a wider range of Te–Te distances,[39] for example, 2.763 (4) Å in $HfTe_5$[45] compared with 4.0 Å (the van der Waals separation) in $HfTe_2$.[1]

In view of these interesting differences, we and other groups have embarked on the elucidation of novel *ternary* tellurides. In the systems M/M′/Te (M = Nb, Ta; M′ = Pt-group metals), a variety of fascinating compounds have already been found: $NbM'Te_5$ (M′ = Ni, Pd),[15,18] $TaM'Te_5$ (M′ = Ni, Pt),[20,27] $Ta_3Pd_3Te_{14}$,[20] $Ta_4Pd_3Te_{16}$,[26] $Ta_4M'Te_4$ (M′ = Fe, Co, Ni as well as Si, Al, Cr),[21] $Nb_2Co_2Te_4$,[17,29] $TaCo_2Te_2$,[29] $M_2Ni_2Te_4$ (M = Nb, Ta),[16,19,28] and $Ta_2Ni_3Te_5$.[28] So far, none of these tellurides is known to have any counterparts among the sulfides and selenides.

The extension of our studies of the M/M′/Te systems to include other late transition metals (M′ = Ru, Os, Rh, Ir) has resulted in new phases ($MM'Te_4$) that are related to the layered binary telluride WTe_2. We report here the crystal and electronic structures of WTe_2,[46] $TaIrTe_4$, and $NbIrTe_4$.[30] On progressing from WTe_2 to $TaIrTe_4$ and $NbIrTe_4$, the metal–metal distances increase and the Te–Te distances decrease. In order to rationalize this structural variation, we have performed band structure calculations with the use of the extended Hückel tight-binding method. Our results suggest that Te–Te bonding is crucial to the stability of the WTe_2 structure type, which is adopted by $TaIrTe_4$ and $NbIrTe_4$, and that electron transfer from the Te^{2-} sp band to the metal takes place. These ideas have been extended to related compounds with different electronic counts in the $MM'Te_4$ (M = Nb, Ta; M′ = Ru, Os, Rh, Ir) series. Indeed, we present some chemical reasons for the competition between metal–metal and

Table I. Crystal Data and Intensity Collection for $TaIrTe_4$ and WTe_2

formula	$TaIrTe_4$	WTe_2
formula mass, amu	883.57	439.05
space group	C_{2v}^7-$Pmn2_1$	C_{2v}^7-$Pmn2_1$
a, Å	3.770 (1)[a]	3.477 (2)[a]
b, Å	12.421 (6)	6.249 (4)
c, Å	13.184 (6)	14.018 (9)
V, Å^3	617.4 (4)	304.6 (3)
Z	4	4
d(calcd), g cm^{-3}	9.50	9.57
T of data collection, K[b]	113	113
radiation	graphite-monochromated Mo Kα (λ(Kα$_1$) = 0.7093 Å)	graphite-monochromated Mo Kα (λ(Kα$_1$) = 0.7093 Å)
μ, cm^{-1}	574.2	572.5
transmission factors[c]	0.187–0.318	0.021–0.216
$R(F^2)$	0.100	0.084
$R_w(F^2)$	0.123	0.117
R (on F for $F_o^2 > 3\sigma(F_o^2)$)	0.049	0.047

[a] Obtained from a refinement constrained so that $\alpha = \beta = \gamma = 90°$. [b] The low-temperature system is based on a design by Huffman.[72] The diffractometer was operated with the use of the Indiana University PCPS system.[73] [c] The analytical method as employed in the Northwestern absorption program AGNOST was used for the absorption correction.[51]

(2) Wilson, J. A. *Phys. Rev. B: Condens. Matter* **1979**, *19*, 6456–6468.
(3) Wilson, J. A.; DiSalvo, F. J.; Mahajan, S. *Adv. Phys.* **1975**, *24*, 117–201.
(4) Ishihara, Y.; Nakada, I. *Solid State Commun.* **1983**, *45*, 129–132.
(5) Ishihara, Y.; Nakada, I.; Suzuki, K.; Ichihara, M. *Solid State Commun.* **1984**, *50*, 657–659.
(6) Suzuki, K.; Ichihara, M.; Nakada, I.; Ishihara, Y. *Solid State Commun.* **1984**, *52*, 743–746.
(7) DiSalvo, F. J.; Rice, T. M. *Phys. Today* **1979**, *32*(4), 32–38.
(8) *Electronic Properties of Inorganic Quasi-one-dimensional Compounds*; Monceau, P., Ed.; Physics and Chemistry of Materials with Low-dimensional Structures Series B; D. Reidel: Dordrecht, Holland, 1985; Parts 1 and 2.
(9) *Crystal Chemistry and Properties of Materials with Quasi-one-dimensional Structures*; Rouxel, J., Ed.; Physics and Chemistry of Materials with Low-dimensional Structures Series B; D. Reidel: Dordrecht, Holland, 1986.
(10) Amberger, E.; Polborn, K.; Grimm, P.; Dietrich, M.; Obst, B. *Solid State Commun.* **1978**, *26*, 943–947.
(11) Biberacher, W.; Schwenk, H. *Solid State Commun.* **1980**, *33*, 385–387.
(12) Ishihara, Y.; Nakada, I. *Solid State Commun.* **1982**, *42*, 579–582.
(13) Fuller, W. W.; Chaikin, P. M.; Ong, N. P. *Solid State Commun.* **1979**, *30*, 689–692.
(14) Gamble, F. R.; DiSalvo, F. J.; Klemm, R. A.; Geballe, T. H. *Science* **1970**, *168*, 568–570.
(15) Liimatta, E. W.; Ibers, J. A. *J. Solid State Chem.* **1987**, *71*, 384–389.
(16) Huang, J.; Huang, B. *Jiegou Huaxue* **1988**, *7*, 214–217.
(17) Huang, B.; Shang, B.; Huang, J. *Jiegou Huaxue* **1988**, *7*, 133.
(18) Liimatta, E. W.; Ibers, J. A. *J. Solid State Chem.* **1988**, *77*, 141–147.
(19) Huang, B.; Huang, J.; Liu, S. *Jiegou Huaxue* **1989**, *8*, 145–148.
(20) Liimatta, E. W.; Ibers, J. A. *J. Solid State Chem.* **1989**, *78*, 7–16.
(21) Badding, M. E.; DiSalvo, F. J. *Inorg. Chem.* **1990**, *29*, 3952–3954.
(22) Keane, P. M.; Ibers, J. A. *Inorg. Chem.* **1991**, *30*, 1327–1329.
(23) Keane, P. M.; Ibers, J. A. *Inorg. Chem.* **1991**, *30*, 3096–3098.
(24) Keane, P. M.; Ibers, J. A. *J. Solid State Chem.* **1991**, *93*, 291–297.
(25) Keane, P. M.; Lu, Y-J.; Ibers, J. A. *Acc. Chem. Res.* **1991**, *24*, 223–229.
(26) Mar, A.; Ibers, J. A. *J. Chem. Soc., Dalton Trans.* **1991**, 639–641.
(27) Mar, A.; Ibers, J. A. *J. Solid State Chem.* **1991**, *92*, 352–361.
(28) Tremel, W. *Angew. Chem., Int. Ed. Engl.* **1991**, *30*, 840–843.
(29) Tremel, W. *J. Chem. Soc., Chem. Commun.* **1991**, 1405–1407.
(30) Mar, A.; Ibers, J. A. *J. Solid State Chem.* **1992**, *97*, 366–376.
(31) Rijnsdorp, J.; Jellinek, F. *J. Solid State Chem.* **1978**, *25*, 325–528.
(32) Meerschaut, A.; Rouxel, J. *J. Less-Common Met.* **1975**, *39*, 197–203.
(33) Hodeau, J. L.; Marezio, M.; Roucau, C.; Ayroles, R.; Meerschaut, A.; Rouxel, J.; Monceau, P. *J. Phys. C: Solid State Phys.* **1978**, *11*, 4117–4134.
(34) Selte, K.; Kjekshus, A. *Acta Chem. Scand.* **1964**, *18*, 690–696.
(35) Bronsema, K. D.; van Smaalen, S.; de Boer, J. L.; Wiegers, G. A.; Jellinek, F.; Mahy, J. *Acta Crystallogr., Sect. B: Struct. Sci.* **1987**, *43*, 305–313.
(36) Meerschaut, A.; Palvadeau, P.; Rouxel, J. *J. Solid State Chem.* **1977**, *20*, 21–27.
(37) *Structural Chemistry of Layer-type Phases*; Lévy, F., Ed.; Physics and Chemistry of Materials with Layered Structures 5; D. Reidel: Dordrecht, Holland, 1976.
(38) Jobic, S.; Deniard, P.; Brec, R.; Rouxel, J.; Jouanneaux, A.; Fitch, A. N. *Z. Anorg. Allg. Chem.* **1991**, *598/599*, 199–215.
(39) Jobic, S.; Brec, R.; Rouxel, J. *J. Solid State Chem.* **1992**, *96*, 169–180.
(40) Canadell, E.; Jobic, S.; Brec, R.; Rouxel, J.; Whangbo, M.-H. *J. Solid State Chem.* **1992**, *99*, 189–199.
(41) Evain, M.; Queignec, M.; Brec, R.; Rouxel, J. *J. Solid State Chem.* **1985**, *56*, 148–157.
(42) Squattrito, P. J.; Swepston, P. N.; Ibers, J. A. *Inorg. Chem.* **1987**, *26*, 1187–1188.
(43) Sunshine, S. A.; Ibers, J. A. *J. Solid State Chem.* **1987**, *71*, 29–33.
(44) Ben Salem, A.; Meerschaut, A.; Guemas, L.; Rouxel, J. *Mater. Res. Bull.* **1982**, *17*, 1071–1079.
(45) Furuseth, S.; Brattås, L.; Kjekshus, A. *Acta Chem. Scand.* **1973**, *27*, 2367–2374.
(46) Brown, B. E. *Acta Crystallogr.* **1966**, *20*, 268–274.

tellurium–tellurium bonding in the ternary tellurides.

Experimental Section

Syntheses. The preparation of the compounds $TaIrTe_4$ and $NbIrTe_4$ has been described previously.[30] Similar synthetic conditions (typically 1000 °C for 1 week) resulted in the preparation of $TaRuTe_4$, $NbOsTe_4$, $TaOsTe_4$, and $TaRhTe_4$, usually as minor phases among a mixture of binary tellurides.

The compound WTe_2 was prepared from a reaction of a stoichiometric mixture of the elemental powders (W, 418 mg, 2.28 mmol, 99.98%, Johnson-Matthey; Te, 582 mg, 4.56 mmol, 99.5%, AESAR) that were ground together and loaded into a quartz tube (12-cm length, 10-mm i.d.). A small amount of $TeBr_4$ (~2 mg/cm^3, 99%, Alfa) was added to serve as a transport agent. The tube was evacuated to 10^{-4} Torr, sealed, and placed in a two-zone furnace. The furnace was heated over a period of 1 day to 820 °C at the hot zone and 700 °C at the cool zone. After the sample was heated for 8 days, it was cooled to room temperature over 1 day. About 75% of the initial charge was found at the cool end of the tube as large black plates or flat needles. A microprobe analysis of several of these crystals with an EDAX- (Energy Dispersive Analysis by X-rays) equipped Hitachi S570 scanning electron microscope confirmed that both the plates and the needles have the same composition, with an average atomic ratio of W:Te = 1.0:2.0. There was no evidence for incorporation of bromine.

X-ray Structure Determination of $TaIrTe_4$. Analysis of rotation and Weissenberg photographs of $TaIrTe_4$ indicated Laue symmetry *mmm* and provided preliminary cell parameters. The systematic extinction ($h0l$, $h+l = 2n + 1$) is consistent with the orthorhombic space groups D_{2h}^{13}-*Pmnm* and C_{2v}^{7}-*Pmn*2_1. The final cell parameters were determined from a least-squares analysis of the setting angles of 44 reflections in the range of $30° < 2\theta(\text{Mo K}\alpha_1) < 40°$ that were automatically centered on a Picker diffractometer. Intensity data were collected at 113 K with the ω scan technique in the range of $2° \le 2\theta(\text{MoK}\alpha_1) \le 62°$ by methods standard in this laboratory.[47] Six standard reflections monitored at intervals of every 100 reflections showed no significant change during the course of data collection. Crystal data and further details of the data collection are given in Table I and Table IS.[48]

All calculations were carried out on a Stardent ST2500 computer with methods and programs standard in this laboratory.[47] Conventional atomic and anomalous scattering factors were taken from the usual sources.[49,50] The intensity data were processed and corrected for absorption effects.[51] The similarity of the Weissenberg photographs indicated that $TaIrTe_4$ is isostructural with $NbIrTe_4$, and so the space group *Pmn*2_1 was chosen and the initial parameters for all atoms in $TaIrTe_4$ were taken from those of $NbIrTe_4$.[30] The structure was refined by least-squares methods, in which the function minimized was $\sum w(F_o^2 - F_c^2)^2$. The reflections equivalent in *mm*2 were averaged to reduce the 7886 measured reflections to 2349 unique reflections; the R index for averaging was 0.083. Of the 238 reflections for which F_c differed by more than 5% between the hkl and $hk\bar{l}$ reflections, 205 of the differences were accounted for by the chosen direction of the polar axis. In the structure there are four metal sites that occupy very similar environments, so there is the possibility of disorder of Ta and Ir positions. We thus tested a model in which the Ta and Ir atoms were allowed to disorder over the four sites; we imposed the constraints that the Ta and Ir occupancies at a given site sum to 1, that the atoms on a given site have the same thermal parameters, and that the overall composition be $TaIrTe_4$, as the Ta:Ir ratio is 1:1 for numerous crystals from EDAX measurements. This refinement resulted in occupancies of 96 (14)% Ta and 94 (14)% Ta in two of the metal sites and 110 (14)% Ir and 80 (14)% Ir in the other two, with reasonable isotropic thermal parameters for all four sites; there was no improvement in the R index (0.049) over that for the ordered model. These results confirm that the metal atoms in $TaIrTe_4$ are ordered in the same arrangement as found in $NbIrTe_4$.[30] The final cycle of isotropic refinement on F_o^2 of 36 variables and 2349 averaged reflections (including those having $F_o^2 < 0$) converged to a value of $R(F_o^2)$ of 0.100. The value for the conventional R index (on F for $F_o^2 > 3\sigma(F_o^2)$) is 0.049. The final difference electron density map shows no features with a height greater than 3.6% of that of an Ir atom. No unusual trends were observed from an analysis of $\sum w(F_o^2 - F_c^2)^2$ as a function of F_o^2, λ^{-1} sin θ, and Miller indices.

(47) Waters, J. M.; Ibers, J. A. *Inorg. Chem.* **1977**, *16*, 3273–3277.
(48) Supplementary material.
(49) Cromer, D. T.; Waber, J. T. In *International Tables for X-ray Crystallography*; Ibers, J. A., Hamilton, W. C., Eds.; Kynoch Press: Birmingham, England, 1974; Vol. IV, pp 72–98.
(50) Cromer, D. T. In *International Tables for X-ray Crystallography*; Ibers, J. A., Hamilton, W. C., Eds.; Kynoch Press: Birmingham, England, 1974, Vol. IV, pp 149–150.
(51) de Meulenaer, J.; Tompa, H. *Acta Crystallogr.* **1965**, *19*, 1014–1018.

Table II. Positional Parameters and Isotropic Thermal Parameters for $TaIrTe_4$ and WTe_2

atom	x^a	y	z	B (Å^2)^b
		$TaIrTe_4$		
Ta(1)	0	0.05399 (10)	0.00413 (18)	0.29 (2)
Ta(2)	0	0.26974 (11)	0.49104 (16)	0.40 (2)
Ir(1)	0	0.53553 (10)	0	0.42 (2)
Ir(2)	0	0.75428 (10)	0.49157 (14)	0.39 (2)
Te(1)	0	0.06480 (17)	0.38968 (21)	0.37 (3)
Te(2)	0	0.19373 (17)	0.85268 (21)	0.42 (3)
Te(3)	0	0.34583 (18)	0.09572 (22)	0.40 (3)
Te(4)	0	0.41420 (19)	0.63910 (23)	0.53 (4)
Te(5)	0	0.56422 (18)	0.39601 (21)	0.42 (3)
Te(6)	0	0.67759 (18)	0.84693 (22)	0.41 (3)
Te(7)	0	0.84921 (18)	0.10784 (20)	0.39 (4)
Te(8)	0	0.89330 (17)	0.64836 (20)	0.34 (3)
		WTe_2		
W(1)	0	0.60062 (9)	$^1/_2$	0.27 (1)
W(2)	0	0.03980 (9)	0.01522 (5)	0.28 (1)
Te(1)	0	0.85761 (15)	0.65525 (7)	0.34 (1)
Te(2)	0	0.64631 (15)	0.11112 (7)	0.32 (1)
Te(3)	0	0.29845 (16)	0.85983 (7)	0.36 (1)
Te(4)	0	0.20722 (16)	0.40387 (7)	0.34 (1)

^{a} All atoms are in Wyckoff position 2a. $^b B = 8\pi^2\langle u^2\rangle$.

Table III. Cell Parameters (294 K) and Volume per Chalcogen in Known $MM'Te_4$ (M = Nb, Ta; M' = Ru, Os, Rh, Ir) Compounds

compd	a (Å)	b (Å)	c (Å)	vol/Te (Å^3)	remarks
$NbOsTe_4$	3.60 (2)	12.63 (3)	13.59 (4)	38.6 (3)	Weissenberg
$NbIrTe_4$	3.768 (3)	12.486 (10)	13.077 (9)	38.45 (5)	Picker
$TaRuTe_4$	3.61 (1)	12.66 (5)^a	13.50 (2)	38.6 (2)	Weissenberg
$TaRhTe_4$	3.78 (1)	12.66 (4)	13.19 (4)	39.4 (2)	powder
$TaOsTe_4$	3.64 (1)	12.62 (2)	13.72 (1)	39.4 (1)	Weissenberg
$TaIrTe_4$	3.77 (1)	12.38 (1)	13.25 (3)	38.6 (1)	Weissenberg

^{a} Obtained by doubling the observed b axis.

X-ray Structure Determination of WTe_2. The structure of WTe_2 was redetermined in order to obtain accurate metrical details for comparison with those of $NbIrTe_4$ and $TaIrTe_4$. The original structure determination was based on photographic data.[46] Rotation and Weissenberg photographs of WTe_2 show patterns similar to those for the $k = 2n$ reflections of $TaIrTe_4$. Possible space groups are D_{2h}^{13}-*Pmnm* and C_{2v}^{7}-*Pmn*2_1. The final cell parameters were determined from a least-squares analysis of the setting angles of 32 centered reflections in the range of $28° < 2\theta(\text{Mo K}\alpha_1) < 40°$. Intensity data were collected at 113 K with the ω scan technique in the range of $2° \le 2\theta(\text{Mo K}\alpha_1) \le 80°$. Six standard reflections monitored at intervals of every 100 reflections were stable during the data collection. Crystal data and further details of the data collection are given in Table I and Table IS.[48]

From the earlier structure determination of WTe_2, we assumed the space group to be *Pmn*2_1.[52] The initial positions for all atoms were determined by direct methods with the program SHELXS86.[53] Absorption corrections and averaging of equivalent reflections were performed as described above. The chosen sense of the polar axis z accounted for 324 of the differences in 445 Friedel pairs for which F_c differed by more than 5% between the hkl and $hk\bar{l}$ reflections. The unexceptional nature of the thermal parameters supports the stoichiometry WTe_2. The final cycle of isotropic refinement on F_o^2 of 19 variables (including an isotropic extinction parameter) and 2122 averaged reflections (including those having $F_o^2 < 0$) converged to a value of $R(F_o^2)$ of 0.084. The value for the conventional R index on F for $F_o^2 > 3\sigma(F_o^2)$ is 0.047. The final difference electron density map shows no features with a height greater than 1.7% of that of a W atom. No unusual trends were obsrved from an analysis of $\sum w(F_o^2 - F_c^2)^2$ as a function of F_o^2, λ^{-1} sin θ, and Miller indices.

Final values of the atomic parameters and isotropic thermal parameters for $TaIrTe_4$ and WTe_2 are given in Table II. Final structure amplitudes for both compounds are given in Table IIS.[48]

X-ray Examination of Other Compounds. The similarity of rotation and Weissenberg photographs of $TaRuTe_4$, $NbOsTe_4$, $TaOsTe_4$, and

(52) We have chosen the standard setting in lieu of the nonstandard one (*Pnm*2_1) used in the original structure determination.[46]
(53) Sheldrick, G. M. In *Crystallographic Computing 3*; Sheldrick, G. M., Krüger, C., Goddard, R., Eds.; Oxford University Press: London, 1985; pp 175–189.

Table IV. Selected Interatomic Distances[a] (Å) and Angles[b] (deg) for WTe_2, $TaIrTe_4$, and $NbIrTe_4$

WTe_2		$TaIrTe_4$		$NbIrTe_4$[c]	
		Metal–Tellurium Distances			
W(1)–2Te(3)	2.698 (1)	Ta(1)–Te(2)	2.646 (3)	Nb(1)–Te(2)	2.659 (6)
W(1)–Te(1)	2.705 (2)	Ta(1)–2Te(8)	2.756 (2)	Nb(1)–2Te(8)	2.755 (5)
W(1)–2Te(2)	2.798 (1)	Ta(1)–2Te(1)	2.830 (2)	Nb(1)–2Te(1)	2.838 (5)
W(1)–Te(4)	2.803 (2)	Ta(1)–Te(7)	2.888 (3)	Nb(1)–Te(7)	2.883 (6)
W(2)–2Te(1)	2.699 (1)	Ta(2)–Te(4)	2.651 (3)	Nb(2)–Te(4)	2.636 (7)
W(2)–Te(3)	2.712 (2)	Ta(2)–2Te(6)	2.755 (2)	Nb(2)–2Te(6)	2.765 (5)
W(2)–2Te(4)	2.800 (1)	Ta(2)–2Te(7)	2.847 (2)	Nb(2)–2Te(7)	2.857 (5)
W(2)–Te(2)	2.802 (2)	Ta(2)–Te(1)	2.875 (3)	Nb(2)–Te(1)	2.886 (6)
		Ir(1)–2Te(5)	2.640 (2)	Ir(1)–2Te(5)	2.633 (3)
		Ir(1)–Te(3)	2.673 (3)	Ir(1)–Te(6)	2.667 (5)
		Ir(1)–Te(6)	2.681 (3)	Ir(1)–Te(3)	2.671 (4)
		Ir(1)–2Te(4)	2.703 (2)	Ir(1)–2Te(4)	2.697 (4)
		Ir(2)–2Te(3)	2.643 (2)	Ir(2)–2Te(3)	2.634 (3)
		Ir(2)–Te(5)	2.676 (3)	Ir(2)–Te(5)	2.673 (4)
		Ir(2)–Te(8)	2.693 (3)	Ir(2)–Te(8)	2.684 (4)
		Ir(2)–2Te(2)	2.706 (2)	Ir(2)–2Te(2)	2.702 (3)
		Metal–Metal Contacts			
W(1)–2W(2)	2.849 (1)	Ta(2)–2Ir(1)	3.069 (2)	Nb(2)–2Ir(1)	3.078 (5)
W(i)–2W(i)[d]	3.477 (2)	Ta(1)–2Ir(2)	3.042 (2)	Nb(1)–2Ir(2)	3.068 (4)
		Ta(i)–2Ta(i)[d]	3.770 (1)	Nb(i)–2Nb(i)[d]	3.768 (3)
		Ir(i)–2Ir(i)[d]	3.770 (1)	Ir(i)–2Ir(i)[d]	3.768 (3)
		Metal–Metal–Metal Angles			
W(2)–W(1)–W(2)	75.21 (5)	Ir(2)–Ta(1)–Ir(2)	76.59 (5)	Ir(2)–Nb(1)–Ir(2)	75.8 (1)
W(1)–W(2)–W(1)	75.21 (5)	Ir(1)–Ta(2)–Ir(1)	75.80 (6)	Ir(1)–Nb(2)–Ir(1)	75.5 (1)
		Ta(2)–Ir(1)–Ta(2)	75.80 (6)	Nb(2)–Ir(1)–Nb(2)	75.5 (1)
		Ta(1)–Ir(2)–Ta(1)	76.59 (5)	Nb(1)–Ir(2)–Nb(1)	75.8 (1)
		Interlayer Tellurium–Tellurium Contacts			
Te(1)–Te(3)	3.977 (2)	Te(1)–2Te(8)	3.734 (3)	Te(1)–2Te(8)	3.704 (5)
Te(1)–2Te(4)	3.916 (2)	Te(2)–Te(4)	3.928 (4)	Te(2)–Te(4)	3.896 (5)
Te(2)–2Te(3)	3.911 (2)	Te(2)–2Te(7)	3.776 (3)	Te(2)–2Te(7)	3.742 (5)
		Te(3)–2Te(6)	3.822 (3)	Te(3)–2Te(6)	3.787 (5)
		Te(4)–2Te(5)	3.886 (3)	Te(4)–2Te(5)	3.858 (5)
		Te(6)–Te(8)	3.746 (3)	Te(6)–Te(8)	3.708 (5)

[a] Additional tellurium–tellurium distances are listed in Table IIIS.[48] [b] Tellurium–metal–tellurium angles are listed in Table IVS.[48] [c] Reference 30. [d] Equal to the *b*-axis length.

Table V. Comparison of Important Structural and Physical Properties in WTe_2, $TaIrTe_4$, and $NbIrTe_4$

	WTe_2	$TaIrTe_4$	$NbIrTe_4$
metal–metal distances (Å)	2.849 (1)	3.042 (2), 3.069 (2)	3.068 (4), 3.078 (5)
shortest Te–Te distances (Å)			
intralayer	3.477 (2)	3.426 (2)	3.415 (4)
interlayer	3.911 (2)	3.734 (3)	3.704 (5)
ρ_{298} (Ω cm)	7×10^{-4} [a]	1.2×10^{-4} [b]	8.1×10^{-5} [b]
ρ_5 (Ω cm)	1×10^{-4} [a]	7.7×10^{-5} [b]	5.3×10^{-6} [b]
$\chi_{measured}$ (emu mol^{-1})	-6.5×10^{-5} [c]	5.6×10^{-4} [b]	1.6×10^{-3} [b]
$\chi_{corrected}$ (emu mol^{-1})	9.7×10^{-5} [c]	8.9×10^{-4} [b]	1.9×10^{-3} [b]
$n(E_F)$ (states eV^{-1} cell^{-1})	1.3	3.4	3.6

[a] Reference 54. [b] Reference 30. [c] This work.

$TaRhTe_4$ suggests that these compounds are isostructural to $TaIrTe_4$ and $NbIrTe_4$. A long-exposure (4 days) Weissenberg photograph of $TaRuTe_4$ showed none of the weak $k = 2n + 1$ reflections expected from the structure of $TaIrTe_4$. This suggests that the metal atoms may be disordered in $TaRuTe_4$. Cell parameters at 294 K for all the ternary tellurides synthesized are listed in Table III. Because crystals of these materials tend to be very mosaic, the cell parameters show some degree of imprecision.

Magnetic Susceptibility. The electrical resistivities of WTe_2, $TaIrTe_4$, and $NbIrTe_4$ and the magnetic susceptibilities of $TaIrTe_4$ and $NbIrTe_4$ have been reported previously.[30,54] WTe_2 has been reported to be Pauli paramagnetic,[55] but, as we were unable to find any numerical values in the literature, we have measured its magnetic susceptibility. Variable-temperature magnetic measurements were made on 61 mg of single crystals of WTe_2 from 5 to 300 K at a field strength of 5 kG with a Quantum Design SQUID magnetometer. The magnetic data were corrected for background contributions from the sample holder over the entire temperature range. At 5 K, the susceptibility of WTe_2 is independent of the magnetic field from 2 to 10 kG.

Results and Discussion

1. Description of the Structures. WTe_2 possesses a layered structure that is a distorted variant of the CdI_2 type, with the layers stacked along the *c* axis. A view down the *a* axis, given in Figure 1a, shows the labeling scheme and the layer stacking. Selected interatomic distances and angles for WTe_2 and $TaIrTe_4$, as well as for $NbIrTe_4$, are provided in Tables IV, V, IIIS, and IVS.[48] The W atoms move toward each other from their ideal octahedral sites to form zigzag chains along the *a* axis with a W–W bond distance of 2.849 (1) Å. A schematic representation of these W–W zigzag chains is shown in Figure 2a.[56]

(54) Kabashima, S. *J. Phys. Soc. Jpn.* **1966**, *21*, 945–948.

(55) Vandenberg-Voorhoeve, J. M. In *Optical and Electrical Properties*; Lee, P. A., Ed.; Physics and Chemistry of Materials with Layered Structures 4; D. Reidel: Dordrecht, Holland, 1976; p 426.

(56) Generally, the metrical details from the present structure determination are similar to those from the earlier one,[46] but the estimated standard deviations are $^1/_5$ as large. The distances found here are generally slightly shorter, perhaps because the data were collected at a lower temperature. The W–W distance (2.849 (1) Å) is only slightly shorter than that reported earlier (2.861 (4) Å).

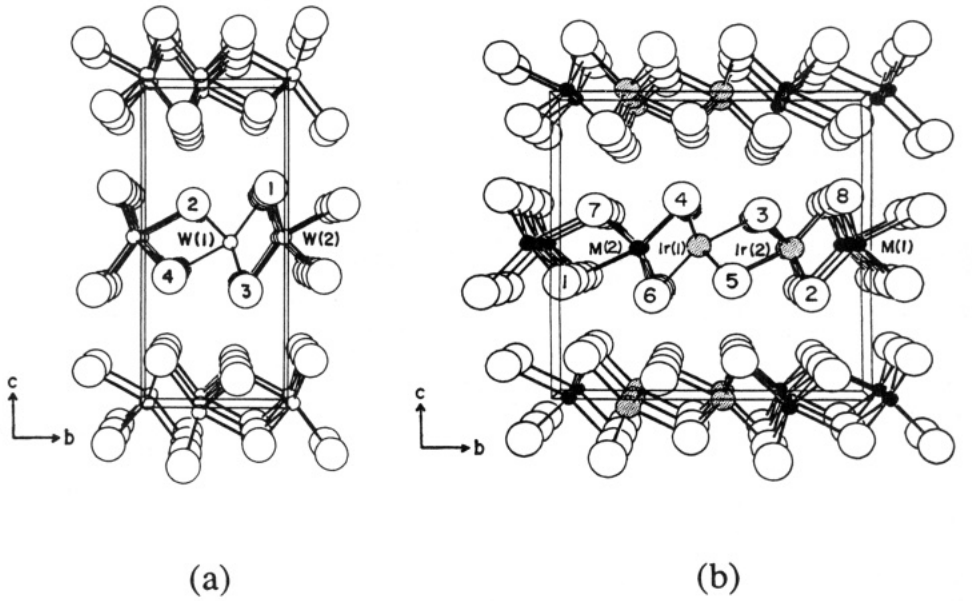

Figure 1. View down the *a* axis of WTe_2 (a) and $MIrTe_4$ (M = Nb, Ta) (b) showing the labeling scheme and unit cell outline. The small open circles are W atoms, the small solid circles are M atoms, the medium stippled circles are Ir atoms, and the large open circles are Te atoms. The metal–metal zigzag chains run down the *a* axis.

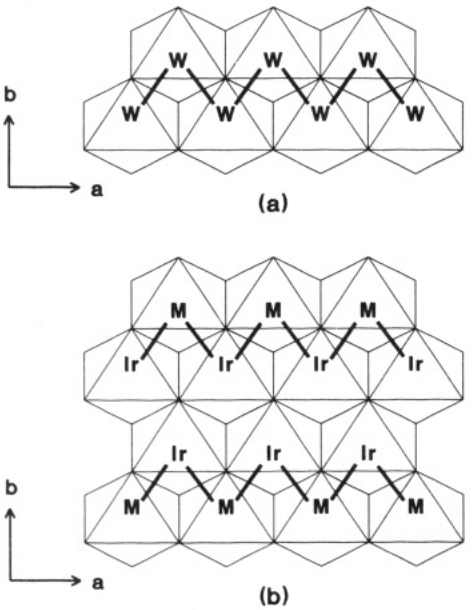

Figure 2. Schematic polyhedral representation of an individual layer viewed down the *c* axis showing the metal–metal zigzag chains running along the *a* direction in WTe_2 (a) and in $MIrTe_4$ (b).

$TaIrTe_4$ is isostructural with $NbIrTe_4$,[30] both of which are derived from the WTe_2 structure, but with a doubling of the *b* axis, as shown in Figure 1b. Again, there are metal–metal chains, but these are constructed from alternating M (M = Nb, Ta) and Ir atoms, as shown in Figure 2b. The zigzag arrangement of metal atoms here is an example of the "metal clustering" that has been observed in other transition-metal chalcogenide systems, in which the particular pattern of clustering is related to the electronic configuration of the metals.[57,58] Moreover, the zigzag chains are ordered in the fashion [M–Ir···Ir–M] when they are linked to form an individual layer, hence the doubling of the *b* axis. Possible reasons for this ordering include charge separation and steric requirements.

As shown in Table IV, the W–Te distances in WTe_2 range from 2.698 (1) to 2.803 (2) Å, roughly corresponding to the sum of the ionic radii of W^{4+} (0.66 Å)[59] and Te^{2-} (2.10 Å).[39] The Ta–Te distances in $TaIrTe_4$ range from 2.646 (3) to 2.888 (3) Å, comparable to those found in $TaTe_2$ (2.663 (8)–2.923 (7) Å);[60] the Nb–Te distances in $NbIrTe_4$ range from 2.636 (7) to 2.886 (6) Å, comparable to those found in $NbTe_2$ (2.690 (7)–2.908 (7) Å).[60] The Ir–Te distances range from 2.640 (2) to 2.706 (2) Å in $TaIrTe_4$ and from 2.633 (3) to 2.702 (3) Å in $NbIrTe_4$, comparable to that found in $IrTe_2$ (2.650 Å).[38] Note that the metal octahedra are not identical in the ternary compounds: the M–Te (M = Nb, Ta) distances show a wider range than do the Ir–Te distances. As Nb and Ta possess identical ionic radii (Nb^{5+}, 0.64 and Ta^{5+}, 0.64 Å; Nb^{4+}, 0.68 and Ta^{4+}, 0.68 Å),[59] it is not surprising to observe that the M–Te (M = Nb, Ta) and Ir–Te distances are comparable in $NbIrTe_4$ and $TaIrTe_4$.

Examination of Table V shows that as we progress from WTe_2 to $TaIrTe_4$ and $NbIrTe_4$, we observe a general trend of increasing metal–metal distances and decreasing Te–Te distances. In WTe_2, the W–W distance (2.849 (1) Å) exceeds that in tungsten metal (2.7411 (3) Å)[61] by 0.11 Å. In $TaIrTe_4$, the mean Ta–Ir distance (3.056 (3) Å) exceeds the average of the metal–metal distances in tantalum and iridium metals (2.8606 (5) and 2.7147 (3) Å, respectively)[61] by 0.27 Å. In $NbIrTe_4$, the mean Nb–Ir distance (3.073 (6) Å) exceeds the average of the metal–metal distances in niobium and iridium metals (2.8585 (3) and 2.7147 (3) Å, respectively)[61] by 0.29 Å. These short metal–metal distances can be attributed to the presence of metal–metal interactions in these compounds (vide infra). Note that the M–M′–M angles are nearly identical in all three structures (~75.8°) (Table IV), suggesting that similar kinds of orbital interactions are operative in these metal–metal bonds.

Correspondingly, as the metal–metal distances increase, some of the Te–Te distances decrease. The shortest intralayer Te–Te distances (from 3.477 (2) Å for WTe_2 to 3.415 (4) Å for $NbIrTe_4$) are considerably less than the van der Waals Te–Te separation (~4.0 Å) and are thus fairly strong interactions. While the intralayer Te–Te distances do not show much variation among the three compounds, there is a clear trend of decreasing interlayer Te–Te separations on progressing from WTe_2 to $TaIrTe_4$ and $NbIrTe_4$ (Table V). The shortest interlayer Te–Te distance is 3.911 (2) Å in WTe_2 (comparable to that found in $HfTe_2$ (~4.0 Å),[1] which possesses a true two-dimensional CdI_2 structure), while

(57) Canadell, E.; Whangbo, M.-H. *Inorg. Chem.* **1990**, *29*, 1398–1401.
(58) Canadell, E.; LeBeuze, A.; El Khalifa, M. A.; Chevrel, R.; Whangbo, M.-H. *J. Am. Chem. Soc.* **1989**, *111*, 3778–3782.
(59) Shannon, R. D. *Acta Crystallogr., Sect. A: Cryst. Phys., Diffr., Theor., Gen. Crystallogr.* **1976**, *32*, 751–767.
(60) Brown, B. E. *Acta Crystallogr.* **1966**, *20*, 264–267.
(61) Donohue, J. *The Structures of the Elements*; Wiley-Interscience: New York, 1974.

these distances are about 0.2 Å shorter in $TaIrTe_4$ (3.734 (3) Å) and $NbIrTe_4$ (3.704 (5) Å). Thus, the two-dimensional character progressively declines on going from WTe_2 to $TaIrTe_4$ and $NbIrTe_4$.

2. Magnetic Susceptibility. The compound WTe_2 displays temperature-independent Pauli paramagnetism, in agreement with its metallic conductivity, with a measured susceptibility of -6.5×10^{-5} emu mol^{-1}. When the contribution from ion-core diamagnetism originating from W^{4+} and Te^{2-} is subtracted,[62] the corrected susceptibility is 9.7×10^{-5} emu mol^{-1}. Table V compares the electrical resistivities and magnetic susceptibilities for WTe_2, $TaIrTe_4$, and $NbIrTe_4$.

3. Band Structure Calculations. We wish to gain insight into the nature of bonding in WTe_2, $TaIrTe_4$, and $NbIrTe_4$ through a comparison of the trends in their structural and physical properties with results from electronic band (extended Hückel) calculations. As WTe_2 and $NbIrTe_4$ represent the extremes in the values of interatomic distances, electrical resistivities, and magnetic susceptibilities (Table V), we focus our attention on these two compounds first. Then we generalize our conclusions to $TaIrTe_4$ as well as other members of the $MM'Te_4$ series. The extended Hückel parameters, given in the Appendix, have been taken from earlier calculations on similar types of compounds (i.e., layered chalcogenides).[57,58,63-65] Although the results of these calculations depend on the initial parameters, we find that chemically reasonable variations in these parameters[66] do not affect the qualitative interpretations that we derive from this very approximate model for bonding in the solid state.

a. Molecular Orbital Calculations on M_2Te_{10} Clusters. The structures of WTe_2 and $NbIrTe_4$ may be constructed from MTe_6 octahedra that are distorted as a result of the formation of M–M bonds. We examine the molecular orbitals first of regular MTe_6 octahedra and then of distorted MTe_6 octahedra and M_2Te_{10} "clusters" with bond distances and angles taken from the crystal structures. This provides an understanding of the influence of the distortion and the metal–metal bonding on the cationic d levels relative to the top of the anionic sp levels. Because the metal d and Te p levels sometimes mix intimately, it is not easy to decompose the atomic contributions to the molecular orbitals. Thus the values obtained from these calculations bear no great significance beyond that of identifying the approximate energies and the relative positions of the d and p levels expected in the real solid.

The results of these calculations are summarized in Figure 3. The t_{2g} levels of W are higher than those of Nb and Ir in the regular MTe_6 octahedra (Figure 3a). When these octahedra are distorted, the Te p levels are raised in energy while the metal t_{2g} levels split slightly in energy (Figure 3b). In the distorted $IrTe_6$ octahedron, the Te p levels are raised high enough so that the Ir t_{2g} levels now lie inside the Te p band that would be expected in the solid. When the two distorted MTe_6 octahedra are edge-shared to form a metal–metal bond and W_2Te_{10} and $NbIrTe_{10}$ clusters (Figure 3c), some of the metal d levels are stabilized. In W_2Te_{10}, the two most bonding W–W levels are 0.9 and 0.5 eV lower in energy than the corresponding levels in the distorted WTe_6 octahedron. Similarly, there is a somewhat smaller stabilization of the Ir d levels in $NbIrTe_{10}$. The Ir d levels are now situated more deeply inside what will be the anionic sp band in the solid, while the Nb d levels are pushed up to levels that are more antibonding. The differences in energy between the top of the anionic sp band (completely occupied if Te^{2-} is assumed) and the lowest unoccupied metal d level in the hypothetical clusters

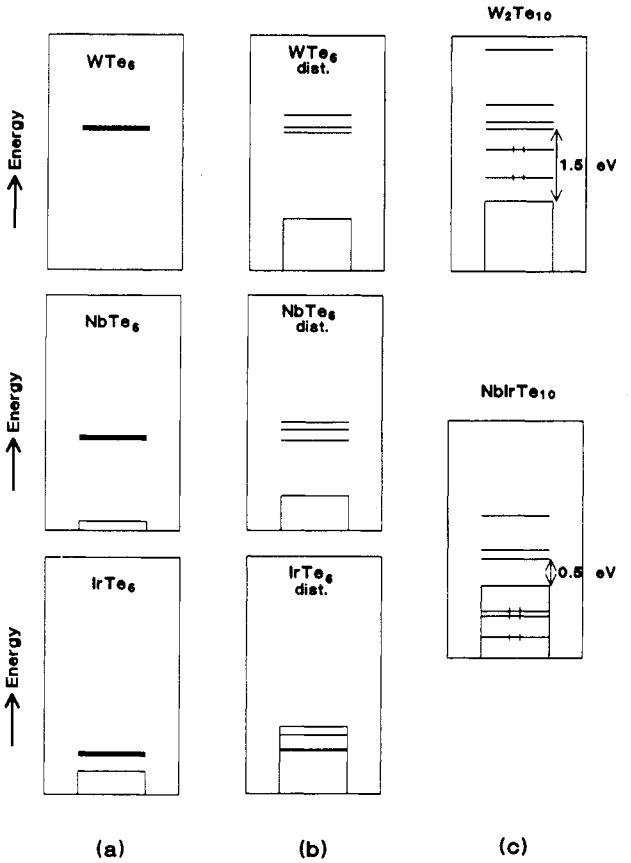

Figure 3. Molecular orbital energies of regular MTe_6 (M = W, Nb, Ir) octahedra (a), distorted MTe_6 octahedra (b), and W_2Te_{10} and $NbIrTe_{10}$ clusters (c). The metal e_g levels are not shown as they are too high in energy to be important in the bonding. In c, the energy differences between the top of the Te band and the first unoccupied d level for $[W_2Te_{10}]^{12-}$ and $[NbIrTe_{10}]^{12-}$ are indicated.

$[W_2Te_{10}]^{12-}$ (W^{4+} d^2) and $[NbIrTe_{10}]^{12-}$ (Nb^{5+} d^0 and Ir^{3+} d^6) are approximately 1.5 and 0.5 eV, respectively. While overlap is unlikely for WTe_2, when the levels of these clusters broaden into bands in the real solids this gap in $NbIrTe_4$ may decrease sufficiently to allow the Te p band and the previously unoccupied metal d band to overlap. Thus, a charge transfer from Te^{2-} to Nb^{5+} is possible as is one from Te^{2-} to Ta^{5+} in $TaIrTe_4$.

b. Band Dispersion in WTe_2 and $NbIrTe_4$. The band structures of WTe_2 and $NbIrTe_4$ along the a^*, b^*, and c^* directions are shown in Figure 4. The Fermi level crosses partially filled bands, in agreement with the metallic conductivity and Pauli paramagnetism of these compounds (Table V). The Fermi level crosses the most disperse bands along the direction ΓX, in accord with the electrical conductivities observed along this direction in these compounds. These bands are constructed essentially from W atomic orbitals in WTe_2 but from a nearly equal mixture of Nb d and Te p atomic orbitals in $NbIrTe_4$, implying that the electrical conductivity along the a direction is mediated entirely through the metal atoms in WTe_2 but through both the metal and Te atoms in $NbIrTe_4$.

In WTe_2, the Fermi level does not cross any bands along the other directions ΓY and ΓZ, corresponding to directions perpendicular to the zigzag W–W chains. But the Fermi level lies within about 0.03 eV of some bands slightly lower in energy, well within the error inherent in the Hückel model. In contrast, in $NbIrTe_4$ the Fermi level crosses one band along ΓY and one band along ΓZ. In the latter direction, corresponding to the stacking axis c, the band crossed by the Fermi level has a significant dispersion (>0.25 eV), implying that there are indeed some interactions between the $NbIrTe_4$ sandwiches, in accord with the rather close interlayer Te–Te distances observed in this structure. This band is constructed essentially from Te atomic orbitals. An oxidation state assignment of Te^{2-} is not possible, for then this

(62) *Theory and Applications of Molecular Diamagnetism*; Mulay, L. N., Boudreaux, E. A., Eds.; Wiley-Interscience: New York, 1976.
(63) Li, J.; Hoffmann, R.; Badding, M. E.; DiSalvo, F. J. *Inorg. Chem.* **1990**, *29*, 3943–3952.
(64) Dedieu, A.; Albright, T. A.; Hoffmann, R. *J. Am. Chem. Soc.* **1979**, *101*, 3141–3151.
(65) Summerville, R. H.; Hoffmann, R. *J. Am. Chem. Soc.* **1976**, *98*, 7240–7254.
(66) Calculations using different Te 5p H_{ii} parameters (−13.20 ± 0.40 eV) were performed. In WTe_2, for example, these variations do not change significantly the relative position of the Fermi level or the general shape of the band dispersion curves.

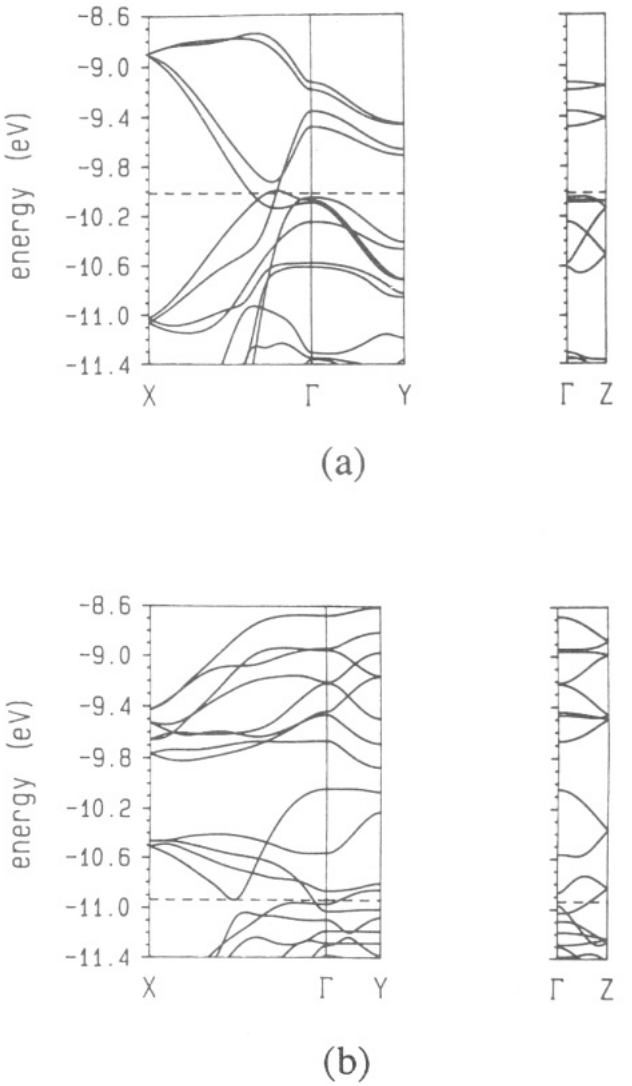

Figure 4. Calculated electronic band dispersion in WTe_2 (a) and $NbIrTe_4$ (b) along a^*, b^*, and c^*. $\Gamma = (0, 0, 0)$, $x = (^1/_2, 0, 0)$, $Y = (0, ^1/_2, 0)$, $Z = (0, 0, ^1/_2)$. The Fermi level is represented by the dashed lines.

band would be entirely filled far beyond the Fermi level. Instead, a Te^{2-} anion will transfer some of its electrons to the lower-lying metallic levels, as sketched in Figure 5.

c. Density of States. The normalized DOS curves extracted from calculations on the three-dimensional WTe_2, $TaIrTe_4$, and $NbIrTe_4$ structures are provided in Figure 6, where the atomic contributions of each element are also shown. In WTe_2, the DOS curve separates into two clearly defined regions of energy: the lower part (below about −11 eV) can be considered to be the Te^{2-} sp band and the upper part to be the cationic d band, and only the metal contributes to the DOS at the Fermi level. In contrast, in $TaIrTe_4$ and $NbIrTe_4$, a large mixing of metal and Te orbitals is observed: this is most clearly seen at the Fermi level, where Te has a considerable contribution (~40%) to the DOS. Thus, in the ternary compounds, Te^{2-} has been partially oxidized. Table V lists the DOS at the Fermi level, $n(E_F)$, to which the magnetic susceptibility of a Pauli paramagnetic compound is directly proportional.[67] The magnetic susceptibility increases in the order $WTe_2 < TaIrTe_4 < NbIrTe_4$, in agreement with the increasing values of the $n(E_F)$. Correspondingly, the compounds are less resistive in the same order.[68]

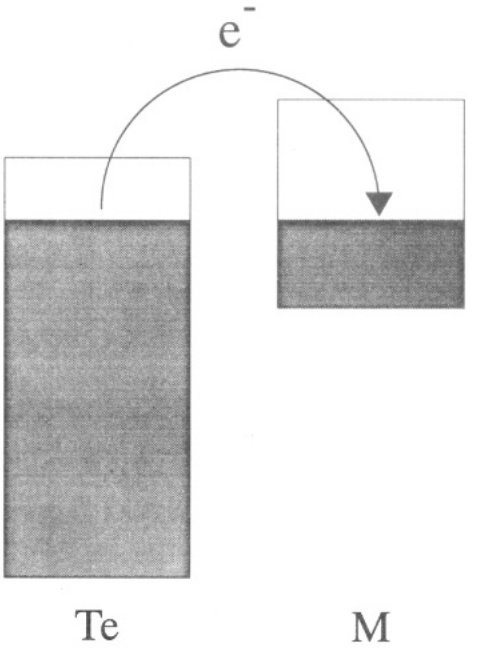

Figure 5. Illustration of the electronic transfer from the Te^{2-} band to the metal d band.

d. Interatomic Distances. Recall the observation of the trends of increasing M–M distances on progressing from WTe_2 to $TaIrTe_4$ and $NbIrTe_4$ (Table V). Because of the different nature of the atoms involved, conclusions about the relative strengths of the W–W, Nb–Ir, and Ta–Ir bonds in these compounds are fraught with danger. Nevertheless, an argument can be made that the *differences* in bond distances are controlled largely by electronic factors. Strengths of different metal–chalcogen bonds have previously been correlated by the valence bond method through the development of a chemically consistent set of valence bond parameters.[69] Given the identical valence bond parameters for M–Te bonds for M = W, Nb, Ta, Ir and the proximity of these elements in the periodic table, it may be feasible to compare the strength of the *metal–metal* bonds in WTe_2, $TaIrTe_4$, and $NbIrTe_4$ through their bond distances, in a first approximation. Note, then, that the expansion of the W–W bond in WTe_2 (2.849 (1) Å) compared with that in the metal (2.7411 (3) Å) (a 4% increase) is considerably less than the expansion of the Nb–Ir bond in $NbIrTe_4$ (3.073 (6) Å) compared with that in the ordered alloy NbIr (2.790 (1) Å)[70] (a 10% increase). It is encouraging that the trend of increasing metal–metal distances is in good agreement with the corresponding decrease in the integrated overlap population (IOPOP)[71] values from 0.27 for WTe_2 to 0.133 for $TaIrTe_4$ and 0.116 for $NbIrTe_4$, although we do not attach significance to the difference in these last two values.

As the M–M distances increase from WTe_2 to $TaIrTe_4$ and $NbIrTe_4$, the interlayer Te–Te distances decrease. The band structure calculations suggest that these variations are controlled by the occupation of electrons in antibonding levels. Figure 7 shows the crystal orbital overlap population (COOP) curves for the metal–metal bonds in these compounds. In WTe_2, a d^2 configuration of the metal is widely accepted, and only the bonding d levels are occupied (Figure 7a).[40] On going from WTe_2 to $NbIrTe_4$ (or $TaIrTe_4$), an additional electron per MTe_2 unit is added. It must occupy an antibonding M–M level as shown in

(67) Ashcroft, N. W.; Mermin, N. D. *Solid State Physics*; Saunders College: Philadelphia, 1976; pp 661–664.

(68) The calculations of $n(E_F)$ were made with a *k*-point mesh of 125; when it is reduced to 27, the qualitative trend remains unchanged. Nor is this trend sensitive to the choice of Gaussian smoothing factor.

(69) Brese, N. E.; O'Keeffe, M. *Acta Crystallogr., Sect. B: Struct. Sci.* **1991**, *47*, 192–197.

(70) Giessen, B. C.; Grant, N. J. *Acta Crystallogr.* **1964**, *17*, 615–616.

(71) The IOPOP of a particular contact is proportional to its strength and is positive for a bonding interaction.

(72) Huffman, J. C. Ph.D. Dissertation, Indiana University, 1974.

(73) Huffman, J. C. Unpublished work.

(74) Hoffmann, R. *Angew. Chem., Int. Ed. Engl.* **1987**, *26*, 846–878.

(75) Whangbo, M.-H.; Hoffmann, R. *J. Am. Chem. Soc.* **1978**, *100*, 6093–6098.

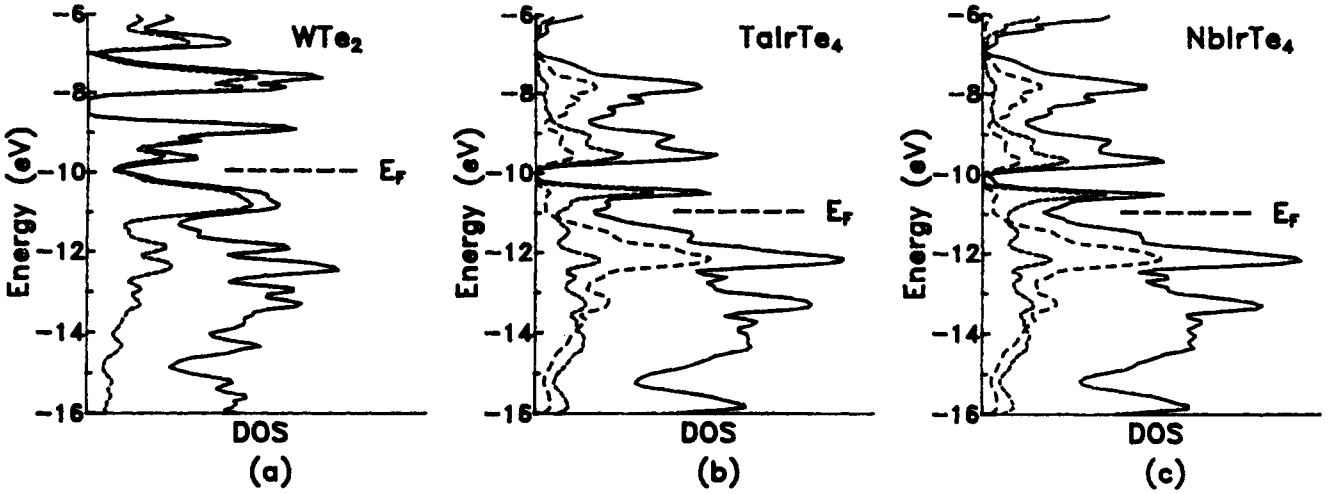

Figure 6. Normalized density of states of WTe_2 (a), $TaIrTe_4$(b), and $NbIrTe_4$(c). The W, Ta, and Nb contributions are represented by short dashed lines, and the Ir contribution is represented by long dashed lines. The Fermi levels are at −10.01 eV for WTe_2, −10.97 eV for $TaIrTe_4$, and −10.94 eV for $NbIrTe_4$.

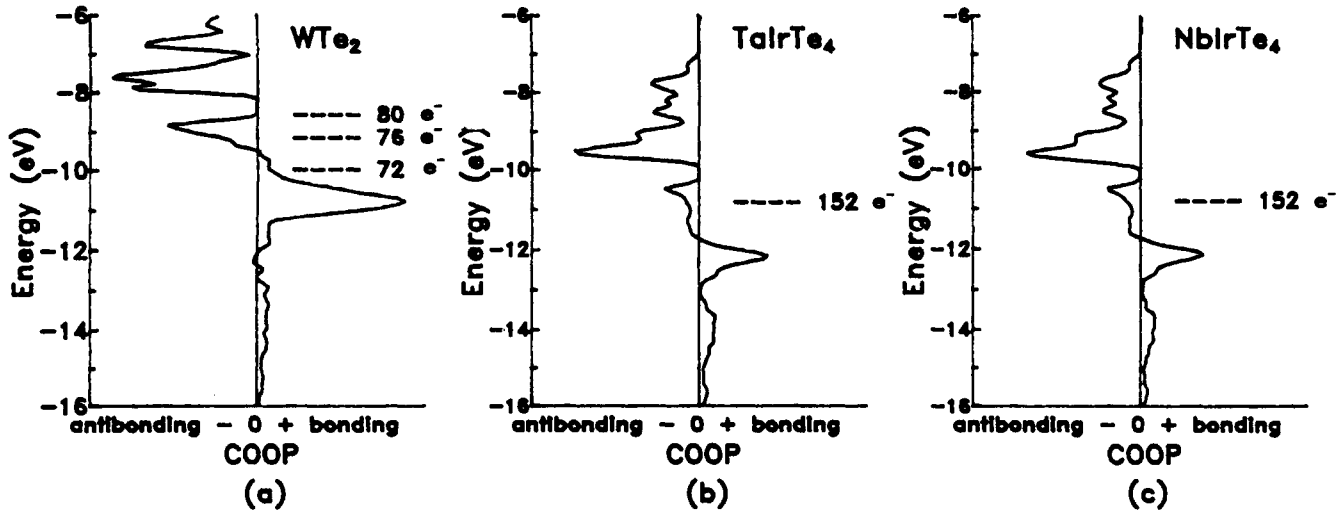

Figure 7. Crystal orbital overlap populations (COOP) curves of the W–W contacts in WTe_2 (a), the Ta–Ir contacts in $TaIrTe_4$ (b), and the Nb–Ir contacts in $NbIrTe_4$ (c). In a, the Fermi levels for d^2 (72 e^-) and hypothetical d^3 (76 e^-) and d^4 (80 e^-) configurations for W are indicated.

Figure 7. Hence, the M–M bond is weakened, and the average M–M distance increases from 2.849 (1) Å in WTe_2 to 3.056 (3) Å in $TaIrTe_4$ and to 3.073 (6) Å in $NbIrTe_4$. Recall that from our previous molecular orbital calculation on the $NbIrTe_{10}$ cluster, we found that Nb d levels lie only slightly higher in energy than the top of the Te p band (Figure 3c). In the real solid, these Nb d levels broaden into bands that overlap considerably with the Te p band, with the result that there is a nearly equal contribution to the DOS from Nb and Te at the Fermi level, as shown in Figure 6c. The Nb d levels cannot remain unoccupied, and there is a redistribution of charge between Te and Nb (as represented earlier in the electron-transfer scheme in Figure 5). In this hypothesis, sufficient electrons are removed from the most antibonding levels in the anionic band, resulting in the formation of some Te–Te bonds. On going from WTe_2 to $TaIrTe_4$ and $NbIrTe_4$, the Te–Te distances generally decrease and many IOPOPs for Te–Te contacts become positive (~0.01 e^-/bond) (Table IIIS).[48] WTe_2 has only one slightly positive IOPOP (0.005 e^-/bond) for a Te–Te contact at 3.477 (2) Å (equal to the *a* parameter) and can be considered to be a true layered compound. We can thus assign formal oxidation states represented by $W^{4+}(Te^{2-})_2$ and assign W the configuration $d^{2+\delta}$ (with δ close to zero).[40]

From the band structure calculations, one can extract an alternative way of assessing electron transfer in the formation of Te–Te bonds in these compounds. By summing the positive IOPOPs for the M–M and Te–Te contacts (multiplied by the number of times they occur in the unit cell) one obtains the total M–M and Te–Te contributions ($M–M_{tot}$ and $Te–Te_{tot}$) to the bonding interactions in the structure. The M–M contribution to the stability of the electronic structure is far greater than the Te–Te contribution in WTe_2 (1.212 vs 0.039), while they are comparable in $TaIrTe_4$ (1.176 vs 0.469) or $NbIrTe_4$ (1.023 vs 0.514). The relative importance of the M–M contribution ($M–M_{tot}/Te–Te_{tot}$) decreases from 31 for WTe_2 (no Te–Te bonding) to about 2 for $TaIrTe_4$ and $NbIrTe_4$ (considerable Te–Te bonding).

e. Net Atomic Charges and Oxidation States. The net atomic charges of each element have been determined from a Mulliken population analysis. Although these values have no chemical significance, they can be compared among isostructural compounds to provide a measure of the extent of electron transfer. The net atomic charge for Te is negative (−0.30) in WTe_2, while it is positive in $TaIrTe_4$ (+0.26) and in $NbIrTe_4$ (+0.28), suggesting that the anionic sp band is far from occupied in the latter two compounds.

The net atomic charges in $TaIrTe_4$ are −1.38, 0.34, and 0.26 and in $NbIrTe_4$ are −1.46, 0.34, and 0.28 for Ta or Nb, Ir, and Te, respectively. These small differences arise because the Ta d levels are higher in energy than the Nb d levels: the overlap between metal d and Te p bands is less and the extent of Te^{2-}-to-metal electron transfer is less in $TaIrTe_4$. Though within the framework of the calculations these differences are not significant, it is interesting that they are consistent with the shorter M–M and generally longer Te–Te distances in $TaIrTe_4$ compared with $NbIrTe_4$. Moreover, electron transfer should take place from Te

Table VI. Extended Hückel Parameters

atom	orbital	H_{ii} (eV)	ζ_1	c_1[a]	ζ_2	c_2[a]
Nb	5s	−10.10	1.89			
	5p	−6.86	1.85			
	4d	−12.10	4.08	0.6401	1.64	0.5516
Ta	6s	−10.10	2.28			
	6p	−6.86	2.24			
	5d	−12.10	4.76	0.6597	1.94	0.5589
W	6s	−8.26	2.341			
	6p	−5.17	2.309			
	5d	−10.37	4.982	0.6685	2.068	0.5424
Ir	6s	−11.36	2.500			
	6p	−4.50	2.200			
	5d	−12.17	5.796	0.6351	2.557	0.5556
Te	5s	−20.78	2.51			
	5p	−13.20	2.16			

[a] Contraction coefficients used in the double-ζ expansion.

to Nb (or Ta) but not from Te to Ir in these compounds.

While the introduction of additional electrons may be thought to destabilize the WTe_2 structure, the chemical system responds by the formation of Te–Te bonds to maintain the stability of the $NbIrTe_4$ or $TaIrTe_4$ structures. Thus, we observe a re-equilibration of electronic energies in which the destabilization of the metal–metal network is partly compensated by the stabilization of the tellurium–tellurium network.

Previously,[30] we suggested the oxidation state formulation $(Nb^{5+})(Ir^{3+})(Te^{2-})_4$. With the band structure calculation now in hand, we find that the Te atoms are not fully reduced. Thus, a better formulation is $(Nb^{4+})(Ir^{3+})(Te^{1.75-})_4$, although it must be viewed with some caution: (1) in a metal, the electrons cannot be as localized as implied by an oxidation state formalism, and (2) the Nb configuration is probably closer to $d^{1-\delta}$. This formulation is intermediate between those proposed for $IrTe_2$ ($Ir^{3+}Te_2^{1.5-}$),[38] which shows extensive Te–Te bonding, and $NbTe_2$ ($Nb^{(4-\delta)+}Te_2^{(2-\delta/2)-}$),[40] which shows much less Te–Te but some metal–metal bonding. Similar conclusions apply to $TaIrTe_4$. Note that the volume per chalcogen in the present ternary compounds ($NbIrTe_4$, 38.45 (5) Å^3; $TaIrTe_4$, 38.59 (3) Å^3) is intermediate between those of $IrTe_2$ (36.12 (1) Å^3)[38] and $NbTe_2$ (39.29 Å^3)[60] or $TaTe_2$ (39.48 Å^3);[60] we interpret this as further evidence for the compromise in a competition between metal–metal and Te–Te bonding.

4. Generalization to $MM'Te_4$ (M = Nb, Ta; M′ = Ru, Os, Rh, Ir). In order to illustrate the influence of the occupation of the antibonding levels on the M–M and Te–Te distances, we have undertaken the syntheses of the other phases $MM'Te_4$ (M = Nb, Ta; M′ = Ru, Os, Rh). Weissenberg photographs reveal that these phases are isostructural with $NbIrTe_4$, and the cell parameters are listed in Table III. The *a* and *c* parameters are directly proportional to the M–M and interlayer Te–Te distances, respectively. As only the *c* parameters vary widely among the different compounds, we examine them to discuss the electronic competition between metal and tellurium.

As the number of d electrons decreases, for example on going from $NbIrTe_4$ to $NbOsTe_4$, electrons are removed from antibonding M–M levels, enhancing metal–metal bonding (shorter *a*) at the expense of Te–Te bonding (longer *c*). On the other hand, as the number of d electrons increases, these electrons must necessarily fill even more antibonding M–M levels, to the extent that the WTe_2-type structure may no longer be favored. Indeed, on progressing from the Ir triad to the Pt triad, the phase $MM'Te_4$ is not formed, but rather a new phase $MM'Te_5$ appears, as exemplified by $TaPtTe_5$.[27]

As the energy of the M′ d levels is raised from $TaRuTe_4$ to $TaOsTe_4$, the extent of Te^{2-}-to-metal electron transfer decreases. To a first approximation, the formulation $Ta^{5+}M'^{3+}Te_4$ (M′ = Ru, Os) seems reasonable. Since the d levels of M′ (with configuration d^5 in this hypothesis) lie inside the Te band, electron transfer will occur from Te^{2-} to M′. This transfer, strengthening the Te–Te bonds, will be greater for Ru than for Os, and so the length of the *c* axis should be less in $TaRuTe_4$ than in $TaOsTe_4$. For $TaRhTe_4$ and $TaIrTe_4$, a transfer from Te^{2-} to M′ (M′ = Rh, Ir) cannot take place because the M′ configuration is d^6, but a transfer from Te^{2-} to Ta is still possible. As the Ir d levels are higher in energy than those of Rh, the difference in energy between the Ta and Ir d levels is less than that between the Ta and Rh d levels, pushing up the Ta–Ir antibonding levels to higher energies than the Ta–Rh antibonding levels. Thus, electron transfer will be more important in $TaRhTe_4$ than in $TaIrTe_4$, and this should lead to a shorter length of the *c* axis for $TaRhTe_4$.

In these compounds, we have noted the importance of the energetic competition between metal–metal antibonding levels and the Te sp band. With a purely d^2 configuration, as in WTe_2, the metal–metal bonds acquire their greatest stability. If more electrons are added to this system, they must necessarily occupy some metal–metal antibonding levels and the stability of the structure decreases. However, the integrity of the structure is maintained through the formation of Te–Te bonds in $MM'Te_4$. That is, what is lost in the weakening of metal–metal bonds is partially regained in the formation of Te–Te bonds. In this process, we progressively lose the two-dimensional character of the structure on going from WTe_2 to $MM'Te_4$.

To elucidate further the trends in the stability of the WTe_2 structure, it would be interesting to intercalate WTe_2 either chemically or electrochemically with Li. Alternatively, it may be possible to effect a progressive substitution of W with a heavier element to increase the electron count.

Acknowledgment. This work was supported by the U.S. National Science Foundation through Grant DMR-88-13623 (to J.A.I.) and DMR-88-09854 (Science and Technology Center for Superconductivity). Use was made of the SEM facilities of the Materials Research Center at Northwestern University (U.S. National Science Foundation Grant DMR-88-21571). We are grateful to Prof. Jeremy Burdett and his group (Dr. John Mitchell and Dr. Theodore Brennan) for assistance in implementing the EHMACC set of programs and to Dr. Michel Evain for providing a band-plotting program. We thank Johnson-Matthey/AESAR for generous loans of Ru, Os, Rh, and Ir powders.

Appendix

The one-electron band structures of WTe_2, $TaIrTe_4$, and $NbIrTe_4$ were calculated from the tight-binding method with an extended Hückel-type Hamiltonian,[74,75] with the use of the atomic parameters listed in Table VI.

Supplementary Material Available: Crystallographic and refinement details (Table IS); integrated overlap populations (IOPOP) in WTe_2, $TaIrTe_4$, and $NbIrTe_4$ for M–M and Te–Te distances shorter than 4 Å (Table IIIS); and selected angles for $TaIrTe_4$ and WTe_2 (Table IVS) (6 pages); observed and calculated structure amplitudes (×10) for $TaIrTe_4$ and WTe_2 (Table IIS) (19 pages). Ordering information is given on any current masthead page.